-

University of Bristol

What happens when wind turbines fall over?

By

Ollie Hanlon
Supervised by Alan Champneys

Department of Engineering Mathematics
University of Bristol

Project thesis submitted in support of the degree of Master of Engineering

April 2022

Abstract

With wind turbines paving the way for a future that needs to be more reliant on renewable energy, this report introduces potential logistical issues of installing new wind turbines on land. These issues are highlighted in a real world case study, where Seabank Power LTD objected the planning application to erect a single turbine by Ambition Community in the Avonmouth region. The reason behind this objection was due to concerns regarding the wind turbine toppling onto a nearby cooling tower and causing damage. Therefore, this report attempts to answer what would exactly happen in such an incident. To do this, a rigid body model is built of the turbine toppling, to calculate the velocity and force of such an impact. The force at impact is calculated to be in a range of 1MN to 14MN, depending on the point of impact along the turbine blade. The turbine blade is then modelled as an inhomogeneous elastic beam to analyse the outcome when subject to an impact load. By calculating the stresses along the blade, it can be determined whether the blade will break and where this break will occur. The results of this model conclude the blade will only break if the point of impact between the blade and the cooling tower is 24m or greater along the blade (for a 40m turbine blade). Furthermore, the point of breaking is likely to occur near the nacelle, rather than the point of impact . Finally a dynamic model is created to analyse the vibrations within the blade after impact. The results of this model show the greatest displacements in the vibrations occur at the tip of the blade, the point of impact and near the root of the blade. This suggests fracture could occur in multiple locations along the blade.

Table of Contents

*

1 Introduction

Tackling climate change is among the top priorities of governments worldwide. In light of the most recent climate change conference, COP26, countries are being asked to secure net zero emissions by the middle of the century [1]. This goal will only be achievable by countries transitioning from their reliance on fossil fuels to renewable energy sources. The UK has already pledged to have enough installed capacity to power all homes through wind energy by 2030, with a £160 million in funding intended for upgrading ports and factories to help build turbines [2].

Wind power is already a huge contributor to the UK energy production, accounting for 24 % of the UK total energy generation in 2020 [3]. Currently offshore wind accounts for 13% and onshore wind for 11%. With large funding from the government and the clear importance to change how we harvest energy, this number is only going to increase. However, development of wind energy has faced its struggles. Since the government ended onshore wind subsides in 2016 [4], there has been a sharp decline in the development of onshore wind farms. In addition to the subsidy cut, local communities tend to oppose plans for onshore turbines [5]. These factors have driven the development of offshore wind farms. In 2020, the UK abandoned its opposition to subsidising new onshore wind farms [4], in the hope to encourage more onshore projects.

The wind energy industry is at the forefront of engineering, pushing the limits of how much energy wind turbines can produce. In 2022 wind turbine manufacturer Vestas will put up a 15MW offshore wind turbine, with a rotary diameter of 236m [6]. With the newer wind turbines getting bigger, in the event of a structural collapse, they may pose a greater risk to life or structures.

Wind turbine collapses are of great concern to the industry. They not only pose a financial threat but can also have a detrimental effect on the ability of developers to install new onshore wind turbines. Perhaps more importantly, they pose a risk to life and property, which will also harm the already fragile public acceptance of new installations. Understanding the cause behind these collapses is vital for creating preventative measures. A study researching previous wind turbines failures found 126 complete collapse events from the year 2000 to 2016, this excludes small turbine under 300KW [7]. The report also states that 55.7% of collapses are due to typhoons and storms, with turbines at greatest risk of failure in the early and late stages of their life cycles. This statistic is worrying considering the projected increase in storm activity in the UK [8].

This report will focus on what exactly happens when a turbine collapses, using a real case study of a planned installation in the Avonmouth area . More specifically the potential damage a wind turbine blade may cause to a civilian structure. With recent controversy of development of onshore wind turbines, understanding exactly the risks of wind turbines may make planning permission easier.

The rest of this report is outlined as follows. Section 2 will contain a review of the relevant literature and introduce the case study that the report will be based upon. This is followed by section 3 which focuses on rigid body modelling of the wind turbine toppling, to calculate the speed and force at impact. Modelling of the wind turbine blade as an elastic beam is undertaken is section 4 in order to evaluate the maximum stresses within the beam at impact. Section 5 evaluates the outcome for various impact conditions, more specifically whether the turbine blade will break or not at impact. Finally, a dynamic beam model is introduced in section 6, which considers how vibrations move throughout the turbine blade in space and time. The results of which are discussed in section 7.

2 Literature review

2.1 Modelling of wind turbine failures

Many papers have looked at the different reasons that lead to a wind turbine failure. Modelling done by J Mayer S Faulstich in [9] identifies different types of failures such as fatigue failures, overload failures and random failures. In contrast Le and Andrews in [10] look at specific sub systems of a wind turbine with the associated risks of failure within each. That paper also states modern wind turbines have around 2000 sensors, with sensors in every subsystem connected to a control system to analyse the condition of wind turbine components. The control system is a huge part of preventing wind turbines from damage, allowing the rotary blades to adjust their pitch, slowing them down at high wind velocities.

There are many papers which have conducted research into wind turbine failures for the purpose of maintenance strategies, see for example [9] [10]. However, it would seem that there are fewer papers have modelled the impacts of a catastrophic failure, where the wind turbines structure undergoes severe damage. Previous studies have modelled the potential impact of a turbines blade detaching from the structure. An M.ENG report by Irvine from 2021 creates a model which is used to simulate different blades' trajectories [11]. By varying different release conditions, he concludes the angular velocity and angle at which the blade is released has the greatest impact on blade trajectories. The results show the furthest thrown blade was 84.29m [11], meaning a large area surrounding the turbine is at potential risk. This modelling was undertaken on turbine with a rotor height of a 100m. A report by MMI engineering attempts to quantify the potential risk of harm to people from wind turbine failures [12]. A combination of simulating a blades flight path with the frequency of failure is used to predict potential harm. Their results show the probability of direct impact by blade/fragment is 10^{-9} per blade thrown, meaning you are more likely to be struck by lightning [12]. However, neither of these reports provide any modelling on what would happen in the case of impact.

In terms of work done on the modelling of what happens when a wind turbine makes impact with the ground or a structure, there appear to few, if any, direct studies. However, this area of contact mechanics is a great concern to other industries such as the automobile industry, where crash analysis has the potential to save many lives. Peter Wriggers book on computational contact mechanics presents the difficulties within this field. To create impact simulations, up to 10 million finite elements are needed for an accurate model [13]. Not only this, but there are multiple contact areas that will undergo either elastic or inelastic deformation upon collision, creating a very non-linear system. Due to the high computational power required to simulate millions of finite elements, this type of analysis is better suited to smaller scale collisions.

Another approach to modelling impact mechanics is via semi analytic methods, where a turbine blade could be potentially modelled as an elastic rod. Modelling how stress waves travel through an elastic rod when impacted with a rigid mass is explained in the book of Johnson [14]. In this incident, the collision causes stress waves to travel through the rod. The events that follow this collision depend on how the mass of the rigid object compares with that of the rod. A light rigid object will be rapidly bought to rest by the compression in the rod. Comparatively, for a heavier object, the pressure wave is reflected up and down the rod many times before being bought to rest. However, this scenario applies strictly for elastic behaviour and inelastic deformation is an important part of real world impacts. Fortunately, inelastic collisions are modelled in chapter 11.5 of [14]. In this chapter the modelling of the impact is dependent on the speed of collision. At moderate speeds of up to 500ms^{-1}, the maximum contact stress, the duration of impact and the coefficient of restitution all need to be determined. The impact behaviour is then dependent on the ratio of kinetic energy absorbed into elastic and plastic deformation in both loading and unloading.

While the modelling of wind turbines impacting the ground is limited, the aerospace industry have undertaken impact tests of a similar scale to wind turbines. These tests are called 'barrel drops', which are vertical drop tests of partial sections of passenger planes. These tests can help evaluate the performance of an aircraft under realistic crash conditions. Such a test was conducted by a joint effort of the National Aeronautics and Space Administration (NASA) and the Federal Aviation Administration (FAA) in 2017 on a a Fokker F28 MK4000 aircraft [15]. The fuselage, containing seats and dummies, was dropped at a pitched angle on a sloped surface to simulate the horizontal velocity of an aircraft in a real crash. A combination of accelerometers on the fuselage, analysis of the soil crater deformation and visual damage to the fuselage were used to evaluate the crash worthiness of the aircraft. While similar drop tests could be an effective way of measuring the damage to wind turbine components in a catastrophic failure, conducting these tests require a lot of resources.

Fortunately, there has been extensive modelling on how wind turbine blades behave under applied loads because of the need to understand how they flex in the wind, see for example [16]

and [17]. Turbine blades are constantly subject to aerodynamic loads, hence structural load analysis is of importance to the wind turbine industry to ensure the blades can withstand these loads. A blade turbine modelled in [16] uses beam theory, where the turbine blade has been modelled as a cantilever beam with a uniformly distributed load. Using this model, local deflections and stresses in the beam can be calculated at any distance. While that paper is only concerned with the distributed loads a wind turbine blade experiences, such a model could be adapted to determine what would happen to the blade subject to a point load in a collision.

2.2 Case Study

In 2020 the planning application by Ambition Community Energy ("ACE") to erect a single turbine in the Avonmouth region was objected by Seabank Power Ltd ("SPL") [18]. SPL own a power station cooling part in close proximity to the desired location of the wind turbine. The objection was due to concerns of the wind turbine toppling onto the cooling plant. To overcome this obstacle, ACE undertook a specific risk assessment of the event to analyse the probability of such an incident [18].

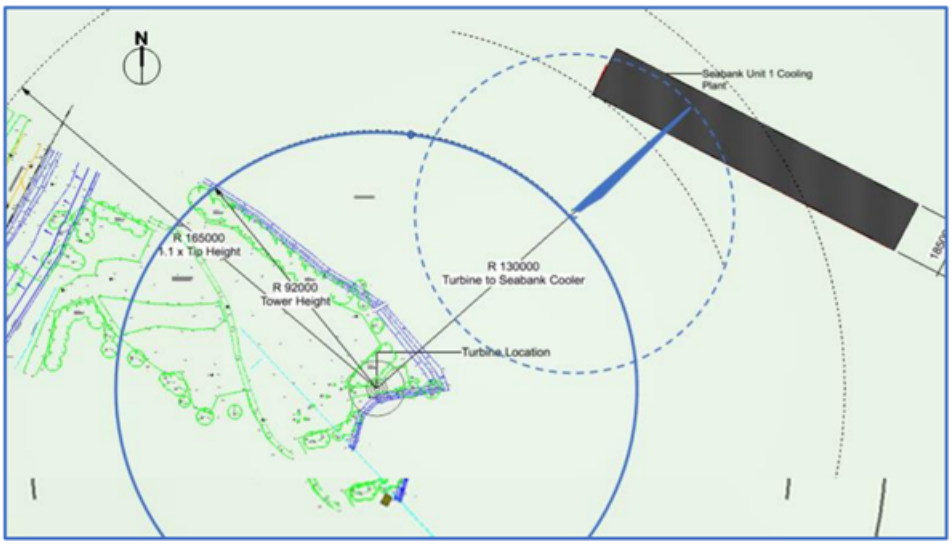

Figure 1: A map showing the distance of the turbine from the cooling plant for the ACE turbine case study, reproduced from [18].

Figure 1 shows that while the turbine tower isn't at risk of toppling onto the cooling plant, the turbine blade is at risk of impact. Analysis of Figure 1 shows that turbine would only make contact with the cooling plant if it fell within a critical band, a sector of angular width of approximately 55° [18]. To determine the likelihood of this event, the report considers the wind conditions of the site and the design conditions of the turbine. The wind speed at the site has an annual mean of 5.7ms^{-1} with an extreme wind of 45ms^{-1}, while the extreme stationary load for the design conditions is 2.4 times than the estimates for the site conditions [18]. Using these

factors the report concludes the probability of a catastrophic failure is 10^{-5} per annum. Then, considering the probability of impact by taking into account the critical band, the probability is calculated to be 2.10^{-6}. While the report does not undertake any detailed evaluation of the damage of such an event, the authors state any damage will be spatially limited due to the high flexibility of the turbine blade reducing the impact load upon collision. This naturally leads to the central question of the report, namely what exactly happens when a turbine blade hits a rigid structure. In more detail, how much load does the blade exert at impact and whether the blade will break.

3 Rigid body model of turbine toppling

In order to understand exactly what happens when a turbine hits the ground or makes contact with a rigid structure, the speed of the collision must be calculated. However, the speed at which the impact occurs is dependent on exactly how the turbine falls over. For example, the turbine could fall face down causing the nacelle to be the point of first contact with the ground. The other scenario is the turbine blade is the point of collision, this would be some form of sideways toppling.

While the proposed turbine for the Avonmouth region is the Enercon E115-EP3 turbine [18], the modelling throughout this report is going to be done on the widely used GE 1.5MW turbine. This decision has been made due to the extensive information regarding the GE 1.5MW turbines specifications that is needed for modelling of the turbine. While this turbine is smaller, having a 77m rotary diameter compared to 115m for the proposed turbine, the turbine is large enough to represent a similar scale collision. The parameters defined in table 1 will be used throughout.

Symbol	Symbol Definition	Value
h_t	height of turbine tower	64.6m
h_n	nacelle radius	2m
m_n	mass of nacelle and rotary system	92000kg
m_t	mass of tower	71000kg
m_b	mass of individual turbine blade	10000kg
L	Length of turbine blade	40m

Table 1: This table shows the variables that are used for modeling of the system. The values of these variables have been found from using a GE 1.5MW wind turbine [19].

3.1 Forwards toppling

Firstly, in the case of forward toppling, the wind turbine has been modelled as a thin beam with mass m_t and a point mass m_n at the end of this beam, as seen in figure 2. The point mass represents the weight of the nacelle and the rotary blades while the rod represents the turbine tower. This system is free to rotate about a hinge at the base of the rod with the turbine height and nacelle radius represented as h_t and h_n respectively.

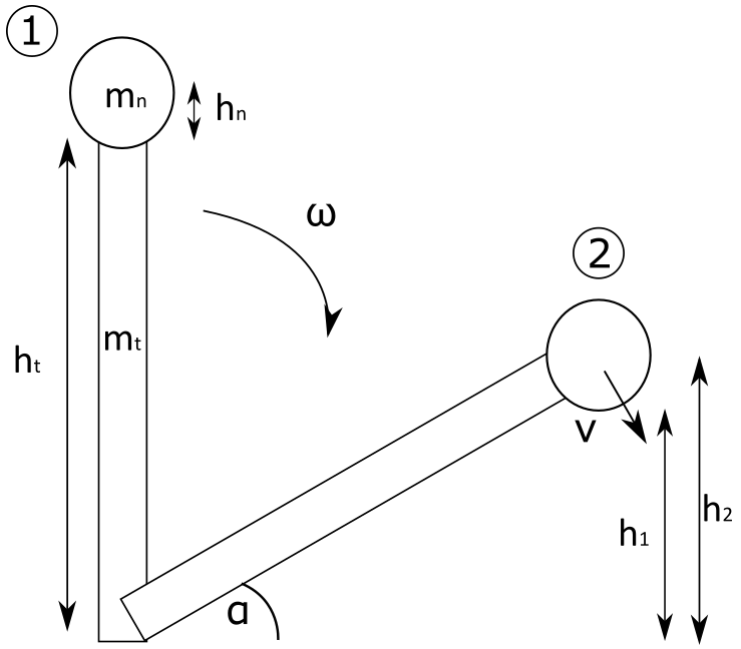

Figure 2: Simplified model of a wind turbine falling, where the turbine at state 1 is at the point of toppling and state 2 is where the turbine would make impact with a structure.

By letting $PE_{i=1,2}$ and $KE_{i=1,2}$ denote the potential and kinetic energy of the system at each state, where state 1 is the upright tower and state 2 is the fallen tower, and assuming the effects of air resistance are negligible. The energy balance equation of the system in its free fall can be written as

$$PE_1 + KE_1 = PE_2 + KE_2, \quad \text{where} \quad KE = \frac{1}{2}I\omega^2 \quad \text{and} \quad PE = mgh, \tag{1}$$

where I, ω, m, g and h represent the moment of inertia, the angular velocity, the mass of the system, the gravitational constant and the height of the system respectively. To create an equation in terms of the variables denoted in figure 2, $PE_{i=1,2}$ and $KE_{i=1,2}$ must be calculated. It is assumed $KE_1 = 0$ and the inertia of the system is measured about the bottom of the rod. Furthermore, to calculate PE_2, h_1 and h_2 from figure 2 must be quantified. Using the sine rule $h_1 = \sin(\alpha)h_t$ and $h_2 = \sin(\alpha)(h_t + h_n)$, where α is the angle the between the turbine and the

ground. By substituting the values $PE_{i=1,2}$ and $KE_{i=1,2}$ into equation (1), the energy balance equation can now be expressed as

$$m_t g\frac{h_t}{2} + m_n g(h_t + h_n) = \frac{1}{2}\big[\frac{1}{3}m_t h_t^2 + m_n(h_t + h_n)^2\big]\omega^2 + m_t g\frac{h_1}{2} + m_n g(h_1 + h_2). \quad (2)$$

To calculate the energy of the system at the point it would hit the ground, it is assumed α is equal to $\frac{\pi}{2}$. Hence, the PE_2 term in equation (1) is equal to 0 and therefore h_1 and h_2 from equation (2) and (3) are also equal to 0. As we are concerned with the velocity at impact, equation (2) can be rearranged for ω, giving

$$\omega = \sqrt{\frac{m_t g(h_t - h_1) + 2m_n g(h_t + h_n - h_1 - h_2)}{\frac{1}{3}m_t h_t^2 + m_n(h_t + h_n)^2}}. \quad (3)$$

Using equation (3) with the parameter values defined in table 1, and assuming the point mass is centered 2m above the tower, ω is calculated at $0.57\text{rad}s^{-1}$ to 2 decimal places. Furthermore, using $v = \omega r$, the velocity at which the top of the turbine hits the ground is equal to 37.962 ms^{-1}. Meaning the kinetic energy upon impact gives 66.29MJ.

3.2 Sideways Toppling

The scenario in which the turbine blade makes contact with the ground first is a bit more complicated. The velocity of the blade striking the ground will be a combination of the blades' velocity from rotating and the velocity of the whole structure falling. To simplify calculations, it is assumed that the tip speed of the blade isn't effected by the whole turbine falling. Carrying on the assumption that the mass of all the turbine blades and the nacelle acts as a point mass, this scenario also assumes that the point mass acts at the top of the turbine tower to reduce the amount of variables in the system.

Figure 3 illustrates the variables of this system. Similar to the case of forwards toppling, ω represents the angular velocity of the structure falling and h_t is the height of the turbine tower. As the turbine blades are now of concern, Ω and L have been introduced to represent the angular velocity of the blades and the blade height respectively. Finally, θ is the angle the turbine blade makes with the ground at the point of collision and h is the vertical distance between the ground and the nacelle. The magnitude of the angle θ will exist in the range of $|\frac{\pi}{6}| < \theta < |\frac{\pi}{2}|$. θ is restricted to this range due to the angle between the blades being fixed at $\frac{2\pi}{3}$, this of course assumes all blades are intact. It must be noted that the blades in Figure 3 are rotating in a clockwise direction. To calculate the velocity at impact, the velocity of the turbine hub and the tip of the turbine blade must be derived ($\hat{v}_h$ and $\hat{v}_b$ respectively). The velocity vectors of these

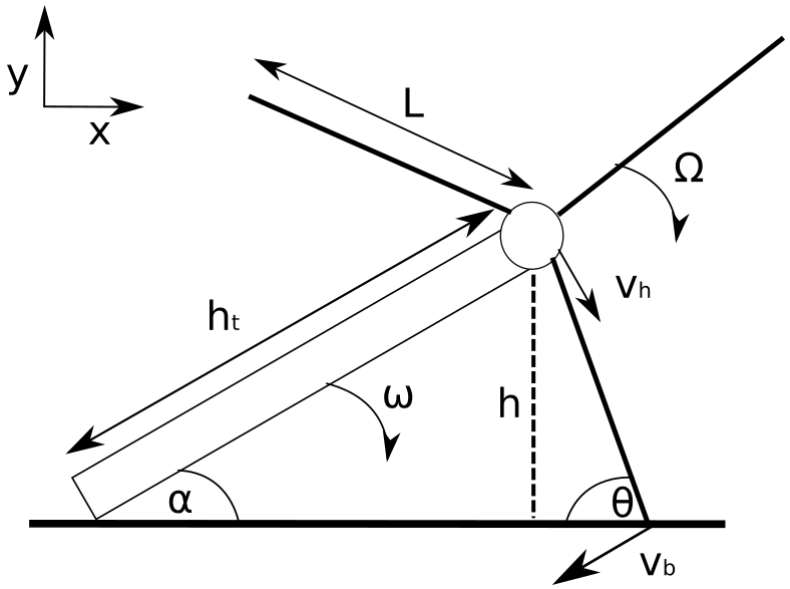

Figure 3: Simplified model of a wind turbine falling onto a turbine blade, illustrating the blade making contact with the ground.

variables can be written as

$$\hat{v}_b = \begin{pmatrix} -L\sin(\theta)\Omega \\ -L\cos(\theta)\Omega \end{pmatrix} \qquad \hat{v}_h = \begin{pmatrix} h_t\cos(\alpha)\omega \\ -h_t\sin(\alpha)\omega \end{pmatrix}. \tag{4}$$

As the circumstances of the collision are dependent on θ, α can be expressed as a function θ by using the sine rule, where

$$\frac{L}{\sin(\alpha)} = \frac{h_t}{\sin(\theta)}. \tag{5}$$

The total velocity of the system is given by the sum of $\hat{v}_h$ and $\hat{v}_b$ and can be expressed by $\hat{v}_{total}$, where

$$\hat{v}_{total} = \hat{v}_h + \hat{v}_b = \begin{pmatrix} h_t\cos(\alpha)\omega - L\sin(\theta)\Omega \\ -h_t\sin(\alpha)\omega - L\cos(\theta)\Omega \end{pmatrix}. \tag{6}$$

Looking at the case where $\theta = \frac{\pi}{6}$, as this is the impact with greatest velocity. It is assumed the wind turbine is in wind conditions where the blade completes 15 rotations in a minute, this is considered an average amount of rotations by wind farms [20]. Hence, Ω can be calculated to be $1.57\text{rad}s^{-1}$ to 2 decimal places. Taking equation (3) from the previous section, h_n and h_2 have been set to 0 due to the assumption that the point mass of the nacelle acts at the

exact height of the turbine tower and $h_1 = \sin(\frac{\pi}{6})L$. Using the dimensions from table 1, the angular velocity of the turbine structure at the point of impact is given as $\omega = 0.15\text{rad}s^{-1}$. By concerning ourselves with strictly the vertical component of velocity at which the blade strikes the ground, the angular velocities of the turbine blade and turbine structure can be substituted into equation (6) with $\alpha = 0.31$ from equation (5). This gives a value of 57.34ms^{-1}, considerably higher than the impact velocity of the forwards toppling scenario.

3.3 Calculating the force exerted on the blade at impact

To evaluate the force at impact, many simplifying assumptions need to be made due to the nonlinear and multiscale nature of impacts. The scenario of the impact has been modelled in figures 4 and 5 , where the cooling tower has been modelled as a spring with height J and the point of impact occurs at a distance δL, where δ is some factor of the blades total length, L. Since the region of the blade that could make impact is small [18], the turbine tower would have almost completely toppled before impact. Therefore to create a simplified situation that is amenable to mathematical modelling, it is assumed at impact between the blade and the cooling tower, the nacelle has just hit the ground. For that reason, the angular velocity of the blade Ω is the sum of the the whole system toppling, calculated in section 3.1 and the blade rotation due to wind. Furthermore in this case, it is assumed that the blade stays attached to the nacelle throughout impact. To further simplify calculations, the blade has been modelled as a uniformly distributed rod, this assumption will be relaxed in the sections below when modelling is done on the deflection of the blade due to impact. Finally it is assumed the maximum force the blade experiences at collision occurs at the point where the spring is at its greatest displacement, as Hooke's law states force is proportional to displacement. This point will occur when the kinetic energy of the system is 0, at this state all the kinetic energy and some of the gravitational potential energy will have been converted into elastic energy.

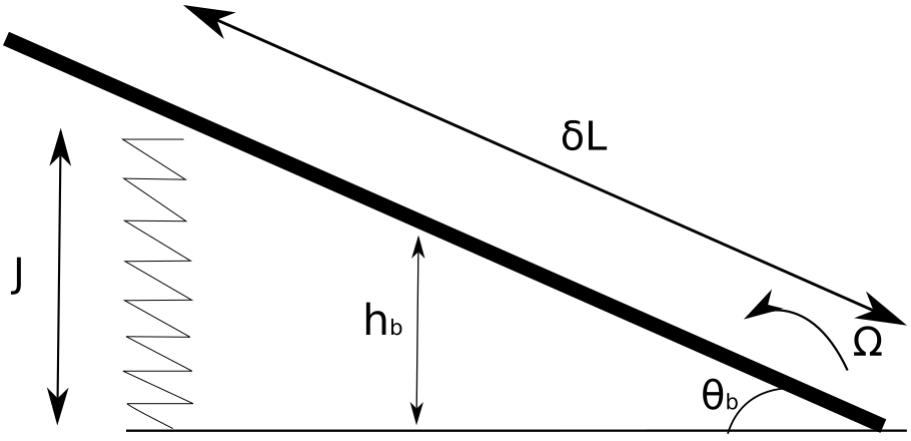

Figure 4: Wind turbine blade system just before impact with cooling tower

The total energy of the system instantaneously before the impact will be the sum of potential and kinetic energy, where the potential energy of the beam will act at the centre of mass of the blade, at a height h_b which is at a distance of $\frac{L}{2}$ along the blade. Therefore, the total energy of the system can be written as

$$T_E = \frac{1}{2}I\Omega^2 + mgh_b, \quad \text{where} \quad h_b = \frac{J}{2\delta} \quad \text{and} \quad I = \frac{1}{3}mL^2\delta^3. \tag{7}$$

h_1 and I have been found using the sine rule and the moment of inertia of a rod respectively.

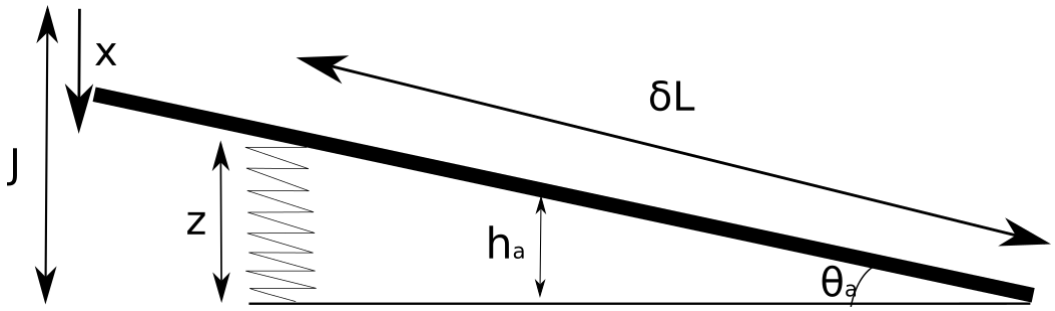

Figure 5: Wind turbine blade system when all the kinetic energy before the collision has been converted into elastic energy

Now considering the system when the kinetic energy of the system is 0, represented by figure 5, the displacement x needs to be defined. By setting the new height of the spring to z, the displacement can be found by

$$x = J - z, \quad \text{where} \quad z = 2h_a\delta \tag{8}$$

and z has be found by using the sine rule. The energy of the system can now be written as a combination of elastic and gravitational potential energy, where it has been assumed that all the energy stays within the system during the collision. Using the substitution of $x = J - 2h_a\delta$, the energy of the system is

$$T_E = \frac{1}{2}k(J - 2h_a\delta)^2 + mgh_a. \tag{9}$$

Considering the case where the point of impact along the blade is known, the only unknown variable needed to calculate the force at impact is h_a . By expanding equation (9) and rearranging for h_a gives

$$h_a = \frac{4J\delta - \frac{2m_bg}{K} \pm \sqrt{(-4J\delta + \frac{2m_bg}{K})^2 - 16d^2(J^2 - \frac{2T_e}{k})}}{8\delta^2} \tag{10}$$

which gives two solutions for h_a. However, the greater value of h_a results in a negative x value, representing when the spring will be in extension after the collision. By concerning ourselves with the smaller value of h_a, the force at impact can be calculated using Hooke's law,

$$F = k(J - 2\delta h_a). \tag{11}$$

Taking the specification of the cooling tower and the wind turbine that is planned to be built [18], the parameters can be set to: $L = 40m, J = 20m$ and $m = 10000kg$. The angular velocity of the blade instantaneously before collision can be calculated by the angular velocity of the system calculated in section 3.1 and the rotation due to wind calculated in section 3.2. Therefore $\Omega = 2.14\text{rad}s^{-1}$. Finally the spring constant associated with the cooling tower needs to be defined. The majority of a cooling towers structure is built with concrete and while concretes elastic properties have not been fully defined, a study has been undertaken to try estimate the spring constant of concrete [21]. By using the method of hammer blowing and analysing the rebound velocity, the report concludes the spring constant, $k = 9.8M\frac{N}{m}$. Using the values of these parameters for values of δ in the range $0 \leq \delta \leq 1$ shows how the impact force is dependent on when the point of collision occurs, as shown in figure 6.

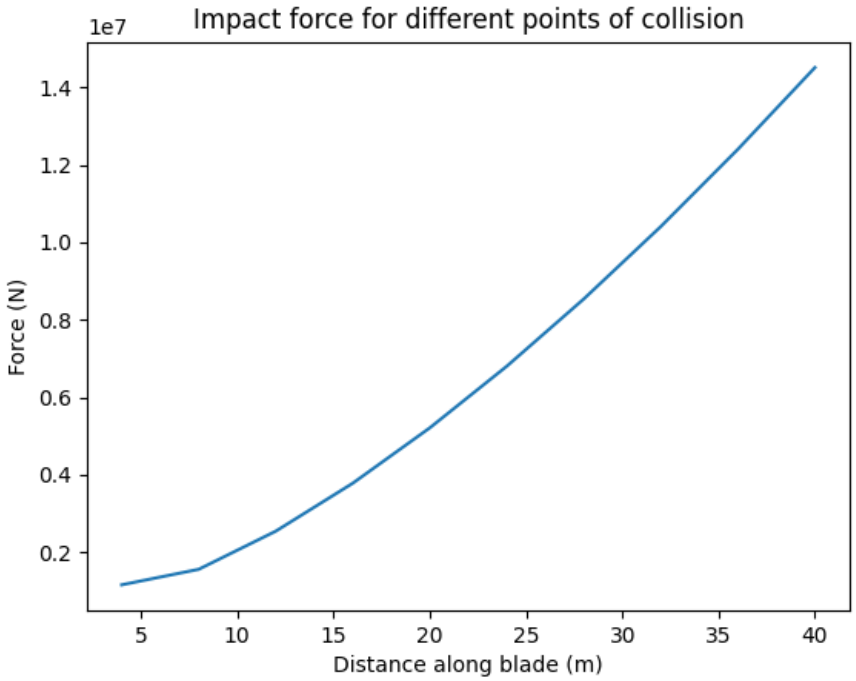

Figure 6: A graph showing how the impact force varies depending on where the point of impact along the blade occurs

Figure 6 clearly shows how the force at impact increases the further along the blade the collision

occurs. This is expected as the moment of inertia increases with distance along the rod, and hence so does the total energy of the system before collision.

4 Elastic Beam Modelling

Taking the example of ACE's plan to erect a wind turbine near a cooling plant, the risk assessment concludes if the wind turbine were to topple, the point of collision would occur somewhere along the turbine blade [18]. Hence to evaluate the outcome of such a collision, the structure of the wind turbine blade needs to be modelled. Since wind turbine blades are continuously subject to applied aerodynamic loads, they are designed to be flexible. An effective way to model how a beam deflects when a static load is applied is to use Euler-Bernoulli beam theory or Timoshencko beam theory. Applying either theory to a wind turbine blade, can give a further insight into what happens to the blades structure under impact.

Since the wind the turbine is attached to the nacelle, the blade can be modelled as a cantilever beam as seen in figure 7, where it is assumed there is no deflection at the fixed end. Furthermore, the blade has been modelled as a frustum to account for the aerodynamic design of the blade.

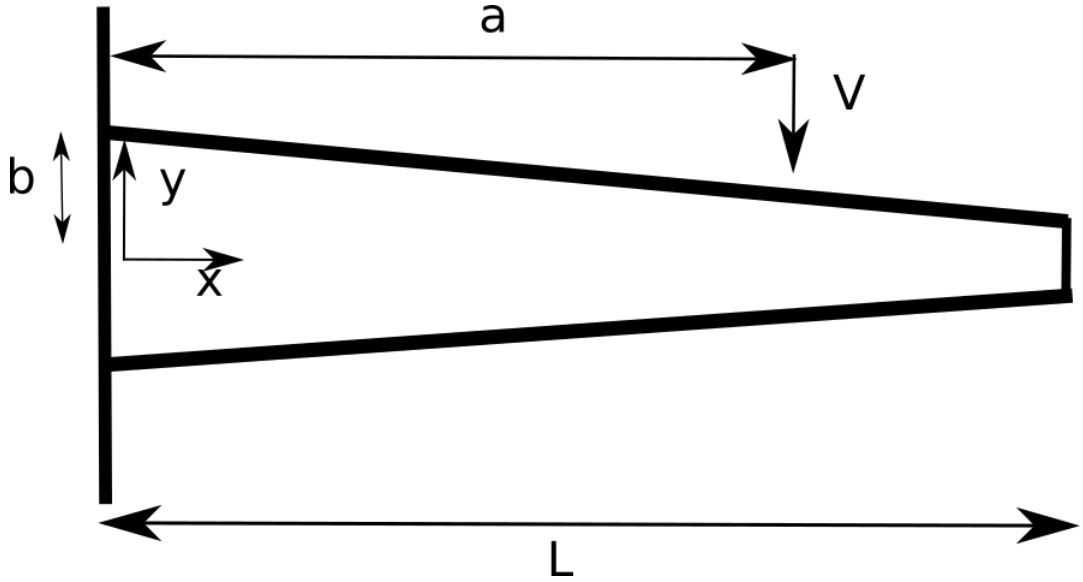

Figure 7: Wind turbine blade modelled as an Euler Bernoulli cantilever beam with a point force applied at a distance a.

It is stated in [16] that the thickness to chord ratio, which compares the maximum vertical thickness of a wing to its chord, is approximately twice the value at the root of the blade then the tip. Therefore, it is assumed that the blades radius in the frustum model is twice the size at the base then the tip. By setting the radius at the base of the frustum to b, the length of the beam to L and assuming the radius at the end is equal to b/2, the cross sectional area can be

calculated at any point along the beam. This is necessary in order to use either beam theories.

4.1 Inhomogeneous Euler Bernoulli Beam

Firstly, modelling the blade as an Euler Bernoulli beam, the effects of shear deformation are ignored. The Euler-Bernoulli beam equation can be used to describe the relationship between the moment along the beam m(x)and the beams deflection y,

$$EI\frac{d^2y}{dx^2} = M(x), \tag{12}$$

where E is the elastic modulus and I is the second moment of area of the beam's cross section. The second moment of area for a circular cross section can be calculated by,

$$I = \int y^2\, dA = \frac{\pi r^4}{4}, \tag{13}$$

where r is the radius of the circle. However, since the blade has been modelled as a frustum, I will vary with distance along the beam. To evaluate how I will vary, the cross sectional area of the beam with respect to distance along the beam needs to be defined. Using the assumption that the radius at the base is twice the size than at the tip of the blade, I can be described by

$$I(x) = \frac{\pi}{4}(b - \frac{bx}{2L})^4, \quad \text{where} \quad r = b - \frac{bx}{2L}. \tag{14}$$

Finally the moment along the beam needs to be defined. Figure 7 represents the scenario of a point load V acting at a distance a along the beam, where there will be a corresponding resultant force and moment acting at the fixed end. The moment when $0 \leq x \leq a$ and $a \leq x \leq L$ can be defined by

$$M(x) = Vx - Va \quad \text{and} \quad M(x) = Vx - Va - V(x-a) = 0 \tag{15}$$

respectively. Taking the former case and subsisting M(x) and I(x) into the Euler-Bernoulli beam equation,

$$\frac{d^2y}{dx^2} = \frac{-4V(x-a)}{\pi E}(b - \frac{bx}{2L})^{-4}. \tag{16}$$

After calculating the integral of equation (11), the derivative of y with respect to x in the region $0 \leq x \leq a$ can be found by,

$$\frac{dy}{dx} = \frac{-4V}{\pi E}\big[\frac{-8L^4}{b^4(2L-x)^2} + \frac{32L^5 - 16L^4a}{3b^4(2L-x)^3} + C_1\big]. \tag{17}$$

Integrating the equation again gives the displacement as a function of distance,

$$y = \frac{-4V}{\pi E}\big[\frac{-8L^4}{b^4(2L-x)} + \frac{16L^5 - 8L^4a}{3b^4(2L-x)^2} + C_1x + C2\big], \tag{18}$$

where C_1 and C_2 are constants of integration. Using the assumption that there is no deflection at the fixed end, the following boundary conditions $y = 0, \frac{dy}{dx} = 0$ at $x = 0$, can be used to calculate the constants of integration, giving $C_1 = \frac{2L(L+a)}{3b^4}$ and $C_2 = \frac{2L^2(4L+a)}{3b^4}$.

Now the case for when $a \leq x \leq L$ needs to be considered. As $M(x) = 0$ in this range, the Euler Bernoulli equation is equal to 0, hence taking the integral of that equation gives,

$$\frac{\partial y}{\partial x} = C3, \quad \text{where} \quad C_3 = \left(\frac{\partial y}{\partial x}\right)_{x=a}. \tag{19}$$

C_3 is equal to the derivative of the beams deflection at $x = a$, therefore it can be calculated by substituting $x = a$ into equation (17). Taking the integral of the previous equation once more gives,

$$y = x\left(\frac{\partial y}{\partial x}\right)_{x=a} + C_4 \tag{20}$$

, where C_4 is calculated by finding the deflection of the beam at $x = a$ and then substituting $x = a$ into the previous equation. Hence,

$$C_4 = y_{x=a} - a\left(\frac{\partial y}{\partial x}\right)_{x=a}. \tag{21}$$

.

Finally the displacement the beam for $a \leq x \leq L$ can be described by

$$y = x\left(\frac{\partial y}{\partial x}\right)_{x=a} + y_{x=a} - a\left(\frac{\partial y}{\partial x}\right)_{x=a}, \tag{22}$$

where

$$\left(\frac{\partial y}{\partial x}\right)_{x=a} = \frac{-4V}{\pi E}\big[\frac{-8L^4}{b^4(2L-a)^2} + \frac{32L^5 - 16L^4a}{3b^4(2L-a)^3} + \frac{2L(L+a)}{3b^4}\big] \tag{23}$$

and

$$y_{x=a} = \frac{-4V}{\pi E}\Big[\frac{-8L^4}{b^4(2L-a)} + \frac{16L^5 - 8L^4a}{3b^4(2L-a)^2} + \frac{8L^3 + 4L^2a + 2La^2}{3b^4}\Big]. \tag{24}$$

This equation describes a linear relationship between displacement and distance along the beam for the region of the beam that lies between the free end and where the point force acts.

4.2 The Timoshencko Beam

Now considering the Timoshencko beam theory, the effects of shear deformation and rotational bending effects are now taken into account. While Euler Bernoulli beam theory assumes that the cross section of the beam is always perpendicular to the neutral axis, Timoshencko assumes it doesn't have to be perpendicular after deformation. Therefore, a new variable φ is used in the Timoshencko beam theory to represent the angle of rotation of the normal to the mid surface of the beam. The equations for the bending moment and the shear force can be defined by

$$M(x) = -EI\frac{d\varphi}{dx} \quad \text{and} \quad V(x) = \kappa AG(-\varphi + \frac{dy}{dx}) \tag{25}$$

respectively, where κ is the Timoshencko shear coefficient, A is the cross sectional area of the beam and G is the shear modulus of the beam. The Timoshencko shear coefficient has not fully been defined, with the coefficient changing depending on whether it is a static or dynamic case. Generally, the coefficient must satisfy the following equation,

$$\int_A \tau \, dA = \kappa AG(-\varphi + \frac{dy}{dx}), \quad \text{giving} \quad \kappa = \frac{6(1+\upsilon)}{7+6\upsilon} \tag{26}$$

for circular cross sections, where τ is the shear stress andυ is Poisson's ratio. This approximation of κ for circular cross sections was derived by Cowper in 1966 [22].

Now focusing on the equations for bending moment and shear force, both are needed to derive an equation of vertical displacement of the beam with respect to distance. By substituting the same bending moment and second moment of area defined in the previous section into the equation of bending moment, then taking the integral, gives

$$\varphi = \frac{-4V}{\pi E}\Big[\frac{-8L^4}{b^4(2L-x)^2} + \frac{32L^5 - 16L^4a}{3b^4(2L-x)^3} + C_5\Big]. \tag{27}$$

Using the Timoshencko boundary conditions that $\varphi = 0$ at $x = 0$, the constant of integration $C_5 = \frac{2L(L+a)}{3b^4}$. Now rearranging the equation of shear force, then substituting the equation for

φ and the area for a circle gives,

$$\frac{dy}{dx} = \frac{V}{\kappa G\pi(b - \frac{bx}{2L})^2} + \frac{-4V}{\pi E}\big[\frac{-8L^4}{b^4(2L-x)^2} + \frac{32L^5 - 16L^4a}{3b^4(2L-x)^3} + \frac{2L(L+a)}{3b^4}\big]. \tag{28}$$

Taking the integral of this equation gives the equation for vertical displacement of the beam

$$y = \frac{2VL}{\kappa G\pi b(b - \frac{bx}{2L})} + \frac{-4V}{\pi E}\big[\frac{-8L^4}{b^4(2L-x)} + \frac{16L^5 - 8L^4a}{3b^4(2L-x)^2} + \frac{2Lx(L+a)}{3b^4}\big] + C_6 \tag{29}$$

where $C_6 = -\frac{2VL}{\kappa G\pi b^2} + \frac{4\upsilon}{\pi E}\big[\frac{2L^2(4L+a)}{3b^4}\big]$ and is calculated from the boundary condition $y = 0$ at $x = 0$. Similar to the equation derived through the Euler Bernoulli beam theory, this equation is only valid in the range $0 \leq x \leq a$ and can be calculated in the range $a \leq x \leq L$ by using the same method of calculating the derivative and displacement of the beam at $x = a$.

4.3 Comparison of static deflection models

To compare the beam models derived, values regarding the wind turbine blades' material properties need to be defined. Since a wind turbine blade is mainly built with fibreglass [16], it will be assumed that the the blade holds the same material properties as fibreglass. The values for the necessary material properties can be found in table 2.

Symbol	Symbol Definition	Value
E	Young's Modulus	72GPa
υ	Poisson's ratio	0.21
G	Shear Modulus	30GPa
b	radius of blade at hub	0.5m
σ	Tensile strength	2GPA

Table 2: This table shows the material properties of the blade, values found from [23]

For both beam models, comparisons will be made when the point force acts at a distance of 30m with a magnitude of 100000N. This is considerably lower than the force the blade would experience at that point of impact, however, an impact of such a force results in deflections greater than the beams length. Deflections of this magnitude are not physically possible and imply the blade will have been destroyed.

As seen in figures 8 and 9 the displacements under the same loading conditions look identical. In fact the difference between the deflection of the beam for both models is no greater than 0.0039m for any point along the blade. This is perhaps due to the extremely high shear modulus of fibre

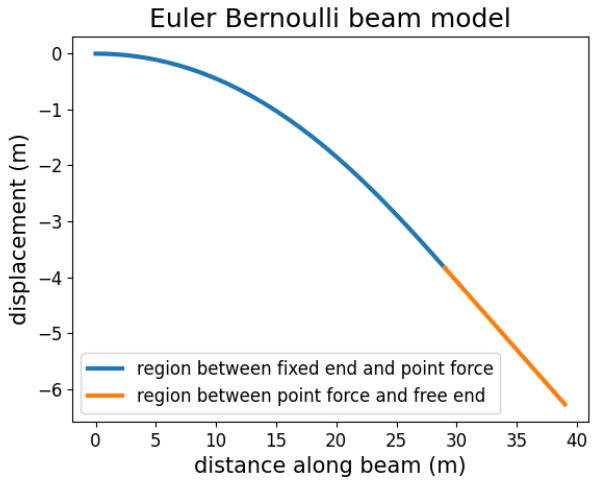

Figure 8: Deflection of Euler Bernoulli beam under a 100000N load at a distance of 30m from the fixed end

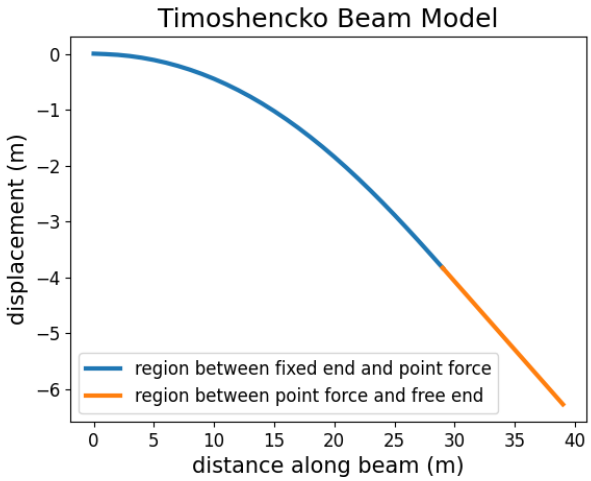

Figure 9: Deflection of Timoshencko beam under a 100000N load at a distance of 30m from the fixed end

glass, which is the materials property to resist shear deformation. Since the Timoshencko model tries to account for the effect of shear deformation and the effects within fibre glass are negligible, it seems more appropriate to use the simpler Euler Bernoulli equation.

4.4 Comparison of homogeneous and Inhomogeneous Euler Bernoulli Beam

In order to evaluate the frustum beam model, comparison will be made with a uniform beam with a circular cross section. For a homogeneous beam, the flexual rigidity is constant throughout the beam, thus the displacement for a homogeneous beam can be calculated using the same method in section 3.1 and is given by

$$y = -\frac{Vx^2}{6EI}(3a - x) \quad \text{between} \quad 0 \leq x \leq a \tag{30}$$

and

$$y = -\frac{Va^2}{6EI}(3x - a) \quad \text{between} \quad a \leq x \leq L. \tag{31}$$

By assuming the homogeneous beams' cross sectional area is equal to the cross sectional at the midpoint of the non homogeneous beam, the displacements for each model under the same impact conditions can be seen in figure 10. Figure 10 shows how when the blade is modelled as a frustum, the blade has greater flexual rigidity nearer the hub, hence deflecting at smaller rate than the uniform beam. Also the maximum displacement is much smaller in the frustum beam

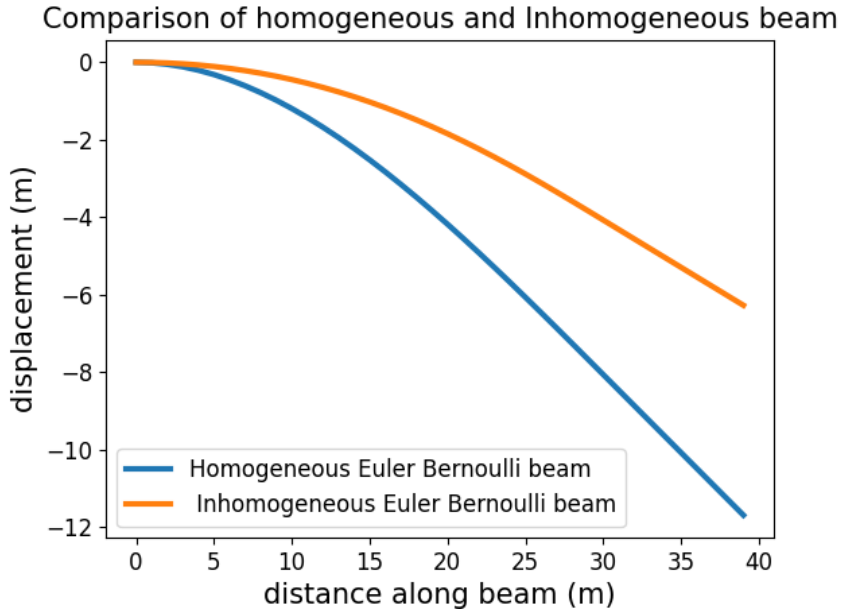

Figure 10: Deflection of homogeneous and Inhomogeneous Euler Bernoulli beam under a 100000N load at a distance of 30m from the fixed end

model, which is expected considering the increased structurally integrity near the hub. While the change in deflection may not be identical to how an actual wind turbine behaves, the model still represents how a wind turbine blade behaviour compares to a uniform beam.

4.5 Stress modelling and failure analysis

In order to analyse what exactly will happen to the beam at impact, the stresses within the beam need to be understood and defined. For a beam with an applied point force in the transverse direction, there are two stresses that are of concern; the bending stress and the shear stress. Bending stress arises due to the material of the beam below the neutral axis being stretched while the over-side is being compressed. This results in maximum bending stress at the surfaces of the beam, while at the neutral axis, the fibres in the beam are neither compressed or stressed. Conversely, shear stress is at a maximum at the neutral axis and is zero at the beams surfaces. Shear stress arises due to the shear force and the direction of stress acts in the same plane as the materials cross section. The bending stress and shear stress can be calculated by

$$\sigma = \frac{M(x)c}{I(x)} \quad \text{and} \quad \tau = \frac{P(x)Q}{I(x)f} \tag{32}$$

respectively, where c is the distance from the neutral axis, $P(x)$ is the shear force, f is the width of the cross sectional area and Q is the fist moment of area bounded by the point of interest

and the surface of the beam. It must be noted that the the equation for shear stress in the beam was derived using the assumption that the width along the beam is constant, for circular cross sections this is only valid at the centre [24]. However, since the maximum stress within the beam is of concern, the shear stress equation can still be used to find the maximum stress at the neutral axis at any point along the beam. In order to calculate the maximum bending stress, the substitution $c_{max} = (b - \frac{bx}{2L})$ is used, as this is the cross sectional radius at any point along the beam and substituting I(x) and M(x) calculated in section 4, the maximum bending stress is

$$\sigma_{max} = \frac{4V(x-a)}{\pi(b - \frac{bx}{2L})}. \tag{33}$$

Since M(x) = 0 for values of $a \leq x \leq L$, the bending stress is equal to 0 in this range. Now focusing on the maximum shear stress at any point along the beam, for a circular cross section the maximum first moment of area is

$$Q_{max} = \frac{2r^3}{3} = \frac{2(b - \frac{bx}{2L})^3}{3}. \tag{34}$$

Finally the shear force needs to be defined, using the Euler Bernoulli equation and equation (11), the shear force is

$$P(x) = -\frac{d}{dx}(EI\frac{d^2y}{dx^2}) = -\frac{d}{dx}(-V(x-a)) = V. \tag{35}$$

By substituting $P(X)$, Q_{max} and the thickness f as the diameter of the beam at any point, the maximum shear stress of the beam can be calculated by

$$\tau_{max} = \frac{4V}{3\pi(b - \frac{bx}{2L})^2}. \tag{36}$$

.

Similar to the bending stress, the shear stress is equal to 0 for values of $a \leq x \leq L$.

By plotting the the maximum shear and bending stress along the blade as seen in figure 11 it is clear the bending stress is considerably greater than the shear stress. The shear stress increases with distance along the blade up until the location of the point force, while the bending stress has an initial increase then tends to 0Pa at the location of the point force. Even though the maximum shear stress seems negligible in comparison, it still has an effect on where the sum of these two types of stresses are greatest along the beam.

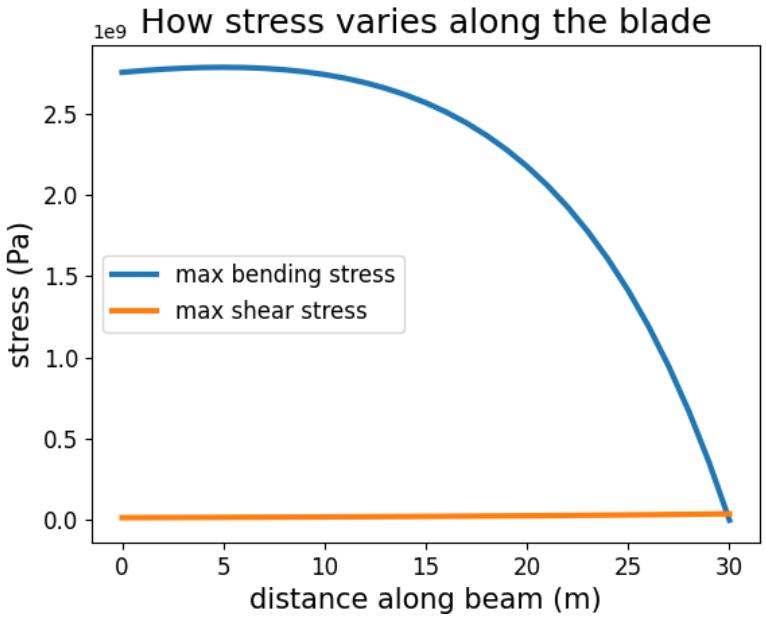

Figure 11: Maximum bending and shear stresses in blade for an impact 30m from the fixed end. Such an impact force will be 9MN.

5 Static Results

Now the maximum stresses within the beam have been defined, it can be determined whether the beam will break under the impact load and where the point of breaking will occur. Firstly, it is assumed that if it any point along the beam, the sum of the bending and shear stress at that point exceeds the ultimate tensile strength of a wind turbine blade, then the blade will break at impact, since ultimate tensile strength is the maximum stress a material can withstand before fracture. Secondly, carrying the assumption that that a wind turbine blade holds the materials properties of fibre glass, the maximum tensile strength of the blade is 2000MPa.

In order to evaluate where the blade will break, it is assumed the breaking point will occur where the sum of the bending and shear stress is greatest along the beam. The outcome of the impact will be simulated for different parameters, including the impact conditions, the blade dimensions and the blades material properties.

5.1 The effects of impact conditions

Since the risk assessment [18] only concludes that in the event of such an impact, the collision will occur somewhere along the blade, results have been produced for different points of impact along the blade to evaluate whether the outcome of the collision changes. The corresponding force for different point of impact has been has been calculated using the results from figure 6.

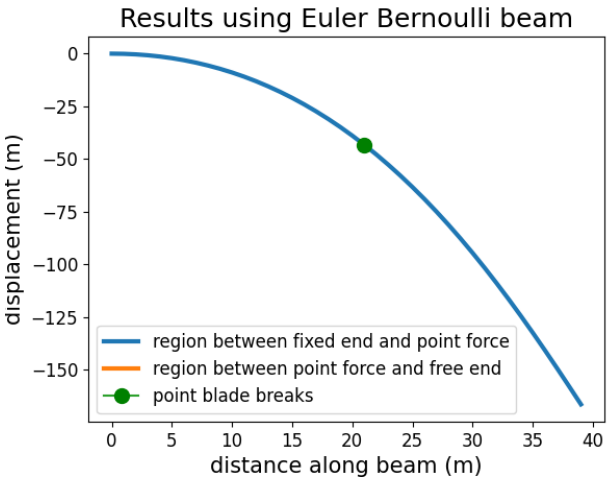

Figure 12: Results of a point force of 14.5MN acting at 40m from fixed end

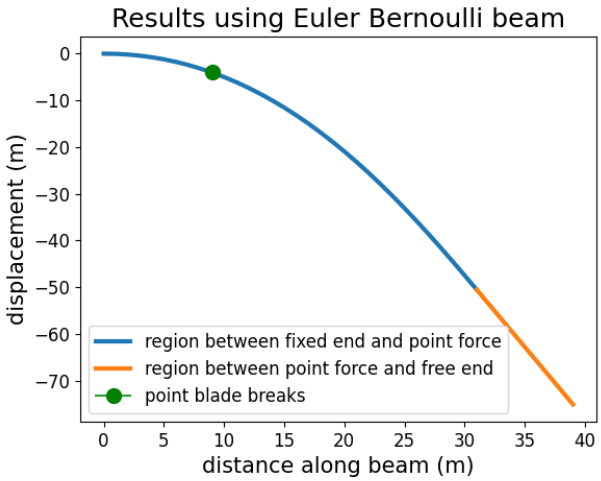

Figure 13: Results of a point force of 10.4MN acting at 32m from fixed end

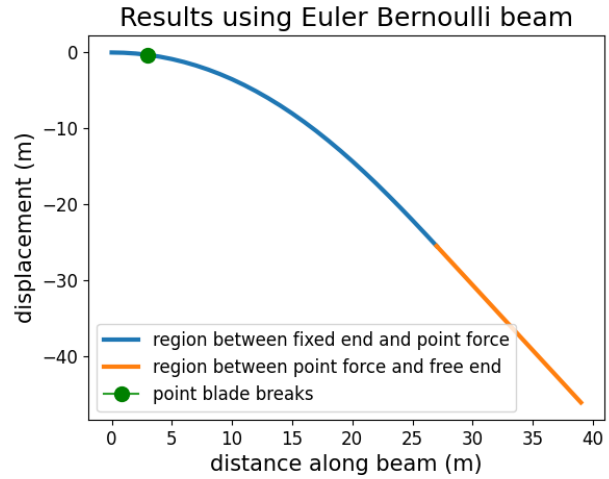

Figure 14: Results of a point force of 8.5MN acting at 28m from fixed end

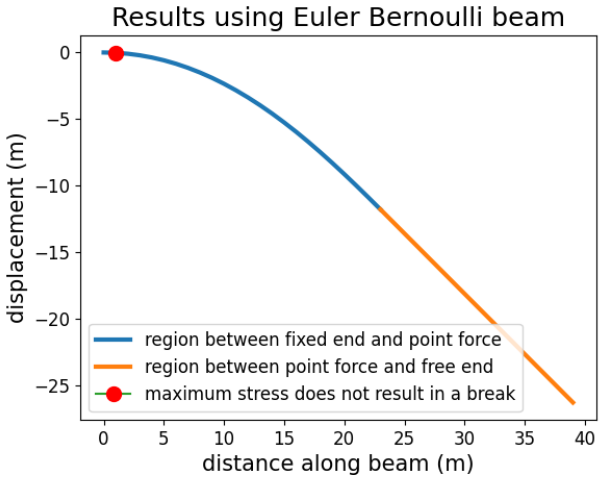

Figure 15: Results of a point force of 6.8MN acting at 24m from fixed end

Figure 12 shows the results of the extreme case where the blade makes impact with the cooling tower at the very tip of the blade. Since the blade has a greater angular kinetic energy at the tip, the force at impact is the largest possible. The Euler Bernoulli model calculates the deflection to be much greater than the blades length and the maximum stress occurs at approximately 20m along the blade, far outweighing the maximum tensile strength. This implies the blade undergoes fracture.

As the point of impact is shifted closer to the fixed end of the blade, the deflection of the blade decreases and the point of maximum stress occurs closer to the hub. Figures 13 and 14 represent this, for impact conditions at 32m and 28m along the blade respectively. Both impacts exceed the maximum tensile strength.

When the point of impact is decreased to 24m along the blade, the maximum stress does not exceed the maximum tensile strength of fibre glass. The Euler Bernoulli model in figure 15 shows how the vertical displacement does not exceed the length of the blade, which is physically possible, given the flexible structural design of turbine blades. Results of all impacts that occur between the fixed end and 24m also do not exceed the maximum tensile strength.

5.2 The effects of blade dimensions

Now considering the blades structural dimensions, the effects of changing the blades thickness or length will be analysed. The parameters regarding the wind turbines radius at its base and the length will be varied for the impact case that the point of collision occurs at a factor of 0.7 of the blades length. This factor is the critical point at which the stresses in the blade are only just greater than the ultimate tensile strength.

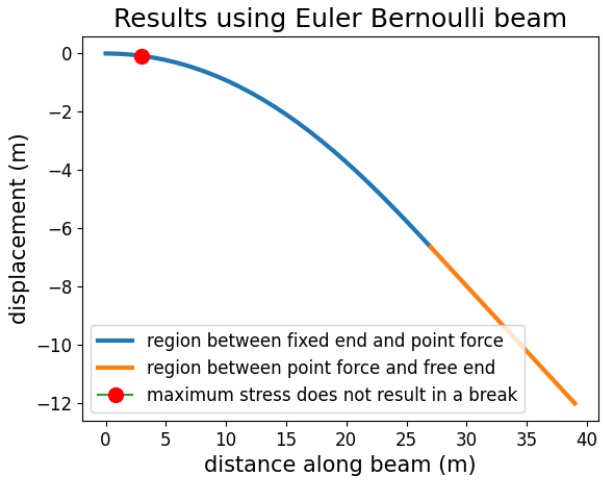

Figure 16: Results of a point force of 8.5MN acting on a blade with a base radius of 0.7m at 28m from fixed end

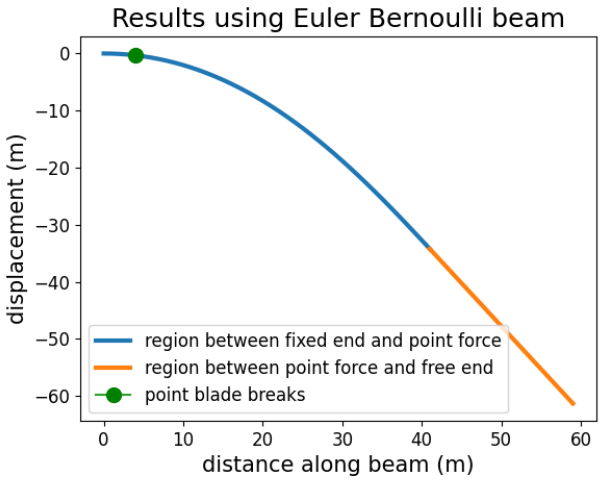

Figure 17: Results of a point force of 12.7MN on a 60m blade with a base radius of 0.7m acting at 42m from fixed end

Firstly, increasing the thickness of the blades base radius to 0.7m has a huge impact on the maximum deflection at impact. Figure 16 shows how the blades deflection at the tip is only 12m, compared to almost 50m for a blade with a 0.5m base radius under the same impact conditions. Clearly, the thickness of the blade has a huge impact on the flexual rigidity of the beam. This is not surprising considering the second moment of area, which represents the ability of a cross sectional area to resist bending, is proportional to the 4th power of the radius of the beam. Moreover, the second moment of area is also inversely proportional to the stresses in the beam, hence the results in figure 16 show how the blade no longer breaks. The maximum stress in the beam is 2.4GPa for a base radius of 0.5m, compared to 1.1GPa when the base radius is 0.7m. Decreasing the blades thickness has the opposite effect, resulting in breaks at lower

impact forces.

To analyse the effects of the blades length, the new force at which impact occurs needs to be accounted for. A longer blade has greater rotational energy nearer the tip, hence resulting in larger impact forces. Considering a 60m wind turbine blade, the impact force at a factor 0.7 of its length is 12.7MN, over 4MN greater a 40m blade in the same conditions. A greater shear force leads to greater stresses in the beam, resulting in a maximum stress of 3.3GPa, far greater than the ultimate tensile strength. On the contrary smaller blades mean there is less kinetic energy in the system, leading to smaller impact forces and hence the blade is less likely to break.

5.3 The effects of material properties

So far all results have been produced assuming the wind turbine blade is made entirely of fibre glass. In reality wind turbine blades are constructed with a variety of materials with stronger materials such as carbon fibre used to reinforce parts of the blade. Some turbine manufactures are even starting to make blades out of wood epoxy, a much more flexible material [16]. The use of different material will not only effect how the blade deflects, but also the maximum stresses it can withstand.

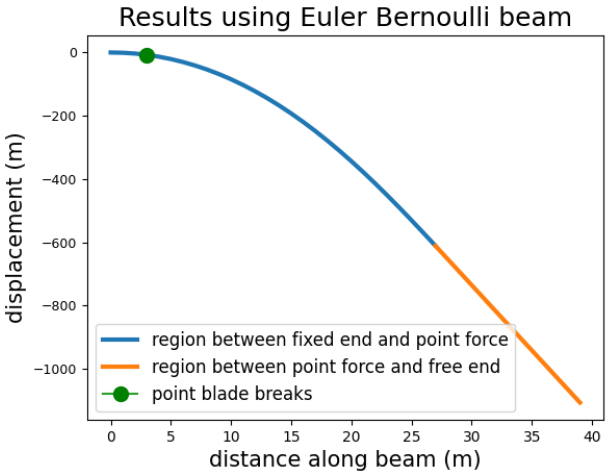

Figure 18: Results of a point force of 8.5MN acting on a wood epoxy blade with a base radius of 0.5m at 28m from fixed end

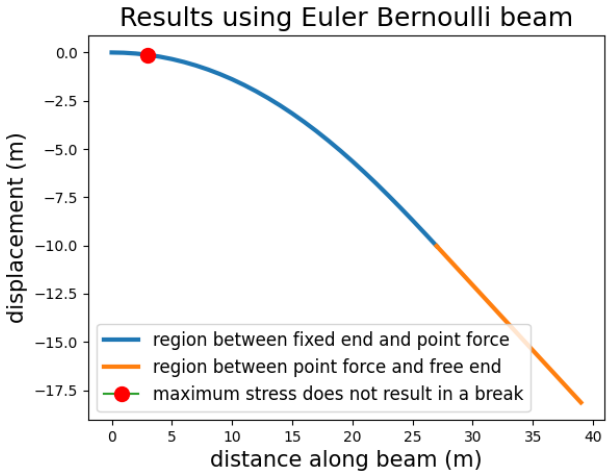

Figure 19: Results of a point force of 8.5MN acting on a carbon fibre blade with a base radius of 0.5m at 28m from fixed end

Taking the case of modelling the turbine blade as purely wood epoxy, the young modulus and tensile strength is approximated to be 950MPa and 30MPa respectively [25]. The results displayed in figure 18 show unrealistic deflections, representing how the flexual rigidity of wood epoxy is much smaller than fibre glass. Even if the blade makes impact with the cooling tower very close to the hub, the blade will still break. It is likely the use of wood epoxy in turbine

blades will be used in cooperation with other materials for structural reinforcement.

On the other hand, the results of a blade entirely made out of carbon fibre in figure 19 experience a maximum deflection of 17.5m, much smaller than 50m for the fibre glass blade under the same impact. Carbon fibres higher Young's modulus and ultimate tensile strength of 150GPA and 3.5GPa respectively [23], mean the blade is much better at resisting bending and only breaks when the point of impact occurs at distances of 36m and greater from the hub.

6 Dynamic beam Equation

So far, all results have been produced for a static scenario, where it was assumed the impact force was applied constantly. To create more realistic results, this assumption will be neglected and instead a scenario where the beam can move in space and time will be considered. This can be done through the dynamic Euler Bernoulli beam equation, which is an extension of simple beam theory [26]. The dynamic beam equation is a partial differential equation and is represented by

$$\frac{d^2}{dx^2}(EI(x)\frac{d^2y}{dx^2}) = -\mu(x)\frac{d^2y}{dt^2} + q(x), \tag{37}$$

where $\mu(x)$ and q(x) is the mass per unit length and the applied force respectively. The equation can be used to analysis the vibration in the beams over time for a given initial condition.

6.1 Cantilever homogeneous Beam

Once again, considering the case where the turbine blade is modelled as a uniform beam, the flexual rigidity and mass per unit length is constant throughout. In addition, the applied force can be set to 0, by instead concerning ourselves with the initial condition that $u(x, 0) = f(x)$. Thus the dynamic beam equation can be simplified to

$$\frac{d^4y}{dx^4} = \frac{-\mu}{EI}\frac{d^2y}{dx^2}. \tag{38}$$

This can be solved through the separation of variables method where the displacement is assumed to be equal to an analytic solution in the form

$$y(x, t) = X(x)T(t), \tag{39}$$

with the following boundary conditions for a cantilever beam:

$$y(0,t) = 0, \quad y'(0,t) = 0, \quad y''(L,t) = 0 \quad \text{and} \quad y'''(L,t) = 0. \tag{40}$$

By substituting equation (39) into equation (38), the PDE can be written as

$$X''''(x)T(t) = \frac{-\mu}{EI}T''(t)X(x) = k, \tag{41}$$

where k is some constant. This equation can then be used to form two separate ODE's in space and time respectively.

6.1.1 Spatial ODE

Firstly considering the spatial ODE

$$X''''(x) - kX(x) = 0 \quad \text{and using the trial solution} \quad X(x) = C_1 e^{\beta x}, \tag{42}$$

4 solutions are found for β. Using the identities that $\sinh x = \frac{e^x - e^{-x}}{2}$, $\sin x = \frac{e^{ix} - e^{-xi}}{2i}$, $\cos x = \frac{e^{ix} - e^{ix}}{2}$ and $\cosh = \frac{e^x + e^{-x}}{2}$ the solution to the spatial ODE can be written as

$$X(x) = A_1 \cos \beta x + A_2 \sin \beta x + A_3 \cosh \beta x + A_4 \sinh \beta x, \tag{43}$$

where A_n, $n \in [1, 4]$ are all arbitrary constants. By applying the boundary conditions defined in the previous section and neglecting the trivial solution $\beta = 0$, we can obtain

$$A_1 = -A_3 \quad \text{and} \quad A_2 = -A_4. \tag{44}$$

This leads to

$$A_1 = -A_2 \frac{\sin \beta L + \sinh \beta L}{\cos \beta L + \cosh \beta L} \quad \text{and} \quad A_1 = A_2 \frac{\sin \beta L + \sinh \beta L}{\cos \beta L - \cosh \beta L}. \tag{45}$$

By equating the two equations derived for A_1, the condition for which β is valid can be found by

$$1 + \cos \beta L \cosh \beta L = 0. \tag{46}$$

There are infinite solutions to equation 46, by denoting the solutions for β as β_n, $n \in \mathbb{N}$ and considering the equations derived for the coefficient A_1, the solution to the spatial ODE can be written as

$$X_n(x) = A_n\Big[\cos\beta_n x - \cosh\beta_n x + \frac{\sin\beta_n L - \sinh\beta_n L}{\cos\beta_n L + \cosh\beta_n L}(\sin\beta_n x + \sinh\beta_n x)\Big]. \tag{47}$$

This equation describes the mode shapes of the beam, which represent the beams deflection pattern for a given natural frequency. Figure 20 represents the mode shapes of the first 4 modes and the sum of them. The sum of all the mode shapes for all solutions of B_n give the actual shape of which the blade will take when vibrating at a natural frequency. It must be noted that A_1 is simply a scaling constant.

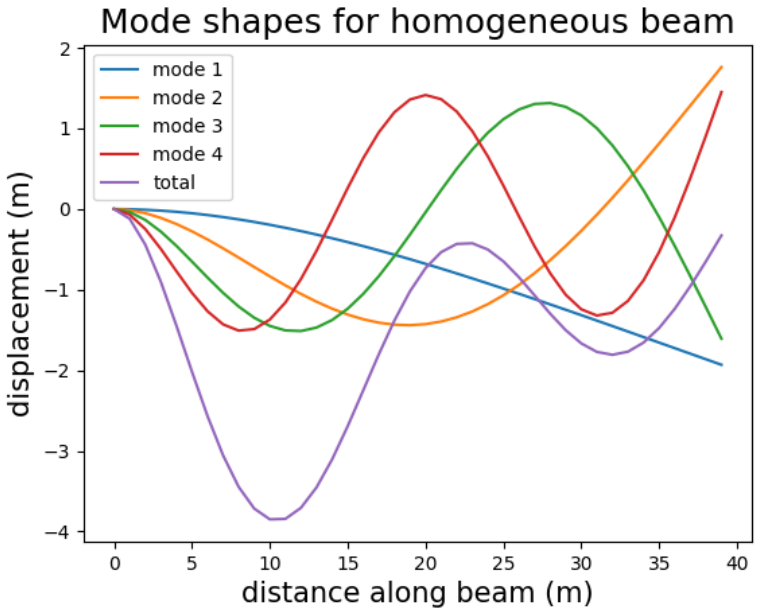

Figure 20: First four mode shapes for a freely vibrating homogeneous cantilevered beam for $A_1 = 1$.

6.1.2 Time ODE

Now paying attention to the ODE derived in time

$$T''(t) + \frac{\beta^4 EI}{\mu}T(t) = 0, \quad \text{and instead using the trial solution} \quad T(t) = C_2 e^{\gamma x}, \tag{48}$$

the solutions found are $\gamma = \pm\sqrt{\frac{EI\beta^4}{\mu}}$. Again using the same trig identities used for the spatial

ODE, the solution to the time ODE can be written as

$$T(t) = B_1 \cos\Big(t\sqrt{\frac{EI\beta^4}{\mu}}\Big) + B_2 \sin\Big(t\sqrt{\frac{EI\beta^4}{\mu}}\Big). \tag{49}$$

However, recalling the boundary condition that $u'(x,0) = 0$, means that $X(x)T'(0) = 0$. This is only the case when the condition $T'(0) = 0$, which is only possible if the constant $B_2 = 0$.

6.1.3 Fitting to initial conditions

Now the solutions to the spatial ODE and time ODE have been derived respectively, the initial assumption that $u(x,t) = X(x)T(t)$ can be used to write the solution of the PDE as

$$y(x,t) = H\Big[\cos\beta x - \cosh\beta x + Z(\sin\beta x + \sinh\beta x)\Big]\cos\Big(t\sqrt{\frac{EI\beta^4}{\mu}}\Big) \tag{50}$$

where,

$$H = A_1 B_1 \quad \text{and} \quad Z = \frac{\sin\beta L - \sinh\beta L}{\cos\beta L + \cosh\beta L}. \tag{51}$$

However, the equation above only considers 1 of the solutions, where the full analytic solution to the PDE is the sum of all possible solutions and can be written as

$$y(x,t) = \sum_{n\in\mathbb{N}} H_n\Big[\cos\beta_n x - \cosh\beta_n x + Z_n(\sin\beta_n x + \sinh\beta_n x)\Big]\cos\Big(t\sqrt{\frac{EI\beta_n^4}{\mu}}\Big). \tag{52}$$

In order to use the solution derived, the coefficients H_n need to be calculated for a given initial condition. By setting the initial condition f(x) to a Dirac delta function, which represent the spike in force applied over a short period of time, f(x) can be written as

$$f(x) = V\delta(x = a), \tag{53}$$

where V is the force at impact and a is the distance from the fixed end at which the force acts. The coefficients H_n can then be calculated by

$$H_n = V\frac{\int_a^L f(x) f_n}{T_n} \tag{54}$$

where f_n represents the mode shapes and T_n is some scaling function which can be calculated

by

$$T_n = \int_a^L fn.fn \; dx. \tag{55}$$

Hence all the coefficients for a given an initial condition can be calculated by the following equation

$$H_n = V \frac{\int_a^L (x-a)(\cos\beta_n x - \cosh\beta_n x + Z_n(\sin\beta_n x + \sinh\beta_n x)) \; dx}{\int_a^L (\cos\beta_n x - \cosh\beta_n x + Z_n(\sin\beta_n x))^2 \; dx}. \tag{56}$$

Since there are infinite mode shapes, solutions to the dynamic beam equation will only be calculated for the first four mode shapes to reduce the number of calculations needed for each result.

6.2 Pinned-pinned homogeneous beam

So far, it has been assumed that the turbine blade behaves like a cantilever beam. In reality the tip of the turbine blade may not be free to move in such a collision, and instead may rest upon the cooling tower. This scenario can be more effectively modelled through a pinned-pinned beam with the following boundary conditions:

$$y(0,t) = 0, \quad y''(0,t) = 0, \quad y(L,t) = 0 \quad \text{and} \quad y''(L,t) = 0. \tag{57}$$

Following the same method of separation of variables used for the cantilever beam but applying the relevant boundary conditions, the condition for which β is valid can be found by

$$\sin(\beta L)\sinh(\beta L) = 0. \tag{58}$$

Since $\sinh(x) \neq 0$, the equation above is satisfied if $\beta L = n\pi$. After applying the boundary conditions for the spatial ODE, the coefficients A_1, A_3 and A_4 are all found to be 0. Hence, after combining the spatial ODE and the time ODE, the full analytic solution to the PDE can be calculated by

$$y(x,t) = \sum_{n\in\mathbb{N}} G_n \sin(\beta_n x)\cos\left(t\sqrt{\frac{EI\beta_n^4}{\mu}}\right), \tag{59}$$

where $G_n = A_3 B_1$. Similar to the cantilever beam, the coefficients G_n can be calculated using the same method in section 6.1.3.

6.3 Inhomogeneous Beam

Moving onto the case where the blade is modelled as a frustum, for a 10000kg blade, the mass per unit length can be defined as

$$\mu(x) = 400 - \frac{3}{40}x. \tag{60}$$

Substituting this and the previously defined second moment of area for the inhomogeneous blade into the dynamic beam equation, we arrive at

$$\frac{d^2}{dx^2}\Big(E\frac{\pi}{4}(b - \frac{bx}{2L})^4 \frac{d^2y}{dx^2}\Big) = -(400 - \frac{3}{40}x)\frac{d^2y}{dt^2}. \tag{61}$$

This equation cannot be solved through the separation of methods and instead requires more complex techniques. While this will not be attempted in this report, it is a possible extension if any further work were to be undertaken on the problem.

7 Dynamic Results

In order to analyse the dynamic response, the solutions has been plotted for 0.1 seconds after the impact, since the damage done to to the blade is likely to occur almost immediately after impact. Plotting the solution for a shorter time period does not capture more than the initial shape the blade takes after impact.

7.1 The effects of load conditions

First considering the impact where the blade hits the cooling tower at 30m from the hub, the dynamic response of the blade can be seen in figure 21. The results show how there are three points of maximum displacement at any given time, with the maximum points of displacements occurring at the tip of the blade, the location of the point of impact and another at approximately 7m from the fixed end.

A similar response can be seen in figure 22 for an impact occurring at 20m from the fixed end. Again three points of maximum displacement can be seen at the tip, the point of impact

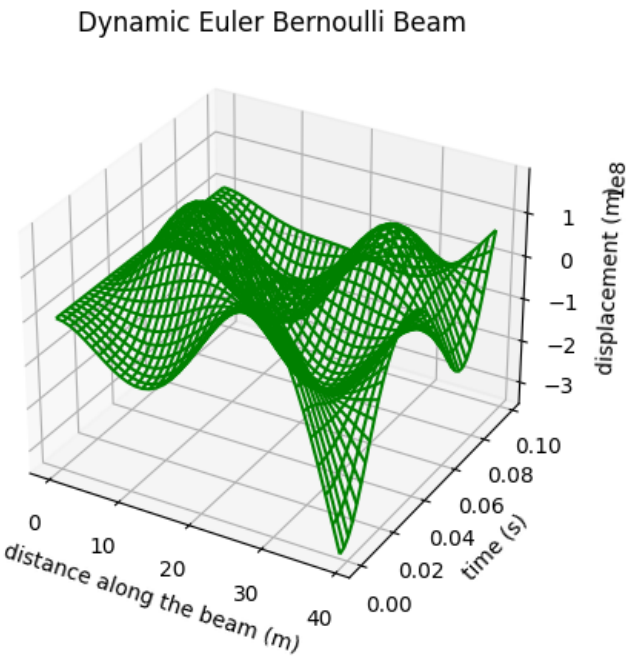

Figure 21: Dynamic response over 0.1s of an Euler Bernoulli cantilever beam subject to an instantaneous 10MN force 30m from the fixed end.

and at around 8m. However, unlike the impact at 30m where the displacement at the tip was much greater than the trough near the fixed end, the maximum displacements are all of similar magnitude in figure 22.

The vibrations within the beam seen in both figures 21 and 22 support the static results to some extent. The static results under the same impact conditions both conclude the maximum point of stress occurs approximately 5m from the hub, about the same distance the dynamic results show the blade is vibrating at a maximum displacement. Nevertheless, the dynamic results also suggest the blade is very unstable at the point of the impact and at the tip.

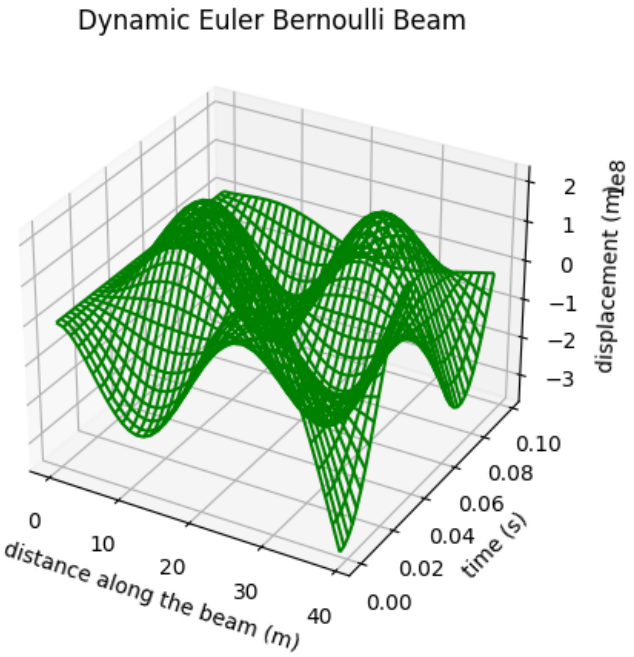

Figure 22: Dynamic response over 0.1s of an Euler Bernoulli cantilever beam subject to an instantaneous 5MN force 20m from the fixed end.

7.2 The effects of material properties

Now considering the effects of modelling the blade as a different material to fibre glass, the results of a carbon fibre blade for impact at 30m along the blade can be seen in figure 23. While the results of a higher Young's modulus blade do not change the locations of the maximum displacements, the blade undergoes more oscillations within the same 0.1 second time period. The same effects are seen when increasing the second moment of area. On the contrary, a lower Young's modulus or second moment of area decrease the speed at which oscillations occur.

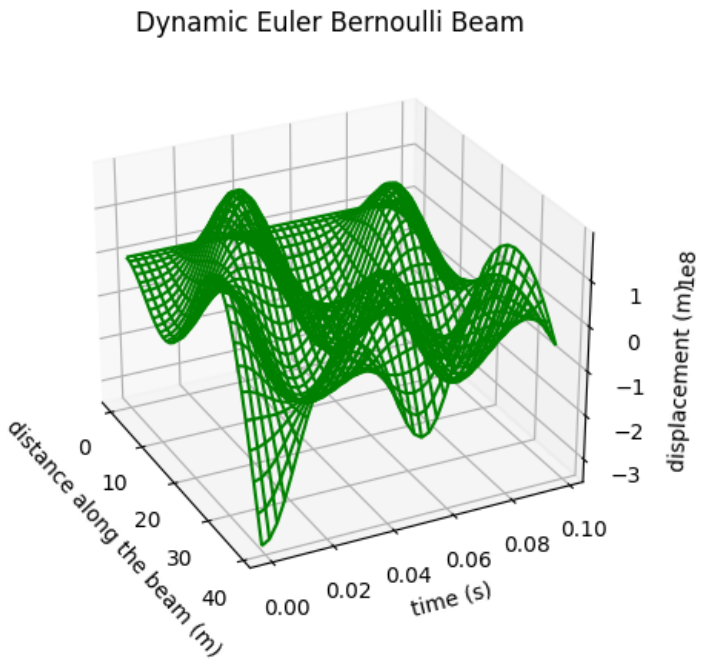

Figure 23: Dynamic response over 0.1s of an Euler Bernoulli cantilever beam subject to an instantaneous 10MN force 30m from the fixed end and modelled as a carbon fibre blade.

7.3 Pinned-Pinned Results

Now focusing on the dynamic response for an elastic beam with pinned-pinned boundary conditions, the results have been plotted over 0.05 second period. This is due to the higher frequency of oscillations for this case, meaning plotting the results over a longer time period results in a cluttered graph, which is difficult to analyse. In comparison to the cantilever case, figure 24 shows the blade undergoing more points of maximum displacement at any given time. Nevertheless, the magnitude of these peaks and troughs are considerably smaller, approximately halve the size. Furthermore, the vibrations seem to travel back and forth along the blade, with the maximum displacement at 32m immediately after impact and then at 5m from the hub 0.04 seconds after the impact. This behaviour is not seen in the cantilever case. Moreover, since the blade is assumed to be resting upon the building after impact, there is no displacement at the tip of the blade. In conclusion, the dynamic response of the pinned-pinned blade shows the vibrations are initially greatest near the point of impact but move close to the hub within a 0.05 second time period.

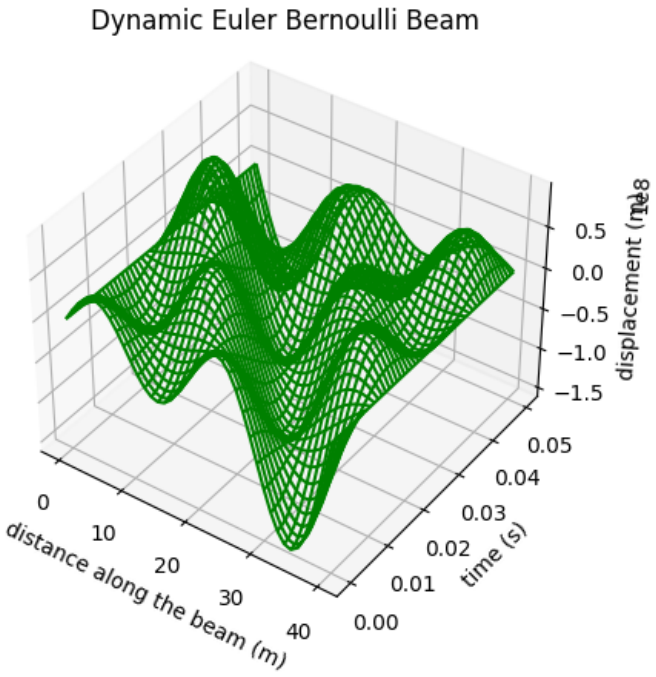

Figure 24: Dynamic response over 0.05s of an Euler Bernoulli pinned - pinned beam subject to an instantaneous 10MN force 30m from the fixed.

8 Conclusion

In this report many simplifying assumptions have been used to analyse the outcome of a wind turbine toppling onto a concrete structure. Simple rigid body mechanics modelling provided an insight into the magnitude of velocity at which such a collision would occur, with an impact velocity between 38 and 57 ms^{-1} depending on how the turbine fell. The velocity calculated was then used to calculate the force at impact, where the collision was modelled as an elastic impact between a spring and a rod. The majority of these calculations involved energy balance equations, where it was assumed that energy was conserved within the system. While this is unlikely to be true in real impact, the calculations will still have provided results of the magnitude expected to see in such a collision. Perhaps the weakest assumption was modelling the building as a spring at impact, given the uncertainty of the spring constant of concrete. Nevertheless, this was an effective way to calculate the force at impact given the non-linearity that would arise in such an impact. The modelling done suggested the impact force could be anywhere in the range of 1MN to 14MN depending on the point of impact along the blade.

Once the impact conditions had been modelled, the turbine blade was modelled as a non homogeneous blade in order to determine the outcome of such an impact. The blade was assumed to be a frustum, to represent the aerodynamic shape of the blade, with a constant Young's

modulus throughout. While the cross section of a turbine blades take the shape of a typical aerofoil, the second moment of area of such a shape is harder to calculate analytically. Even though the modelling of the flexual rigidity in the blade has its limitations, the frustum model still created results of deflections much more representative of how a real turbine blade would bend then modelling of a homogeneous blade. To improve the flexual rigidity modelling, the effects of a non constant Young's modulus could be explored. The assumption that the blade is made entirely of fibre glass is slightly weak considering the blades are created to have enhanced structural integrity in certain places [16].

In terms of evaluating the outcome of the impact, results were produced through stress failure analysis. By calculating the maximum bending stress and shear stress at any given point along the blade, the blade was determined to break if the maximum point of the stresses exceeded the tensile strength of fibre glass. The results suggested the blade was likely to undergo a catastrophic failure near the root of the blade, rather than the point of impact, with the results concluding the blade would break if the collision occurred at 24m or greater from the fixed end. Moreover, the effects of the blade dimensions, particularly the radius of the blade, had a huge impact on whether the stresses in the blade exceeded the tensile strength, changing the base radius by just 0.1m changed the outcome of the collision. This highlights the importance of realistic blade modelling to produce accurate results. Furthermore, all these results were created assuming the impact force was an applied point force. Therefore, the maximum points of stress may occur at different locations in a real impact.

In order to challenge the assumption the impact force is applied constantly, a dynamic beam model was introduced. By solving the PDE for the impact force applied over a short period of time, a 3D plot could be produced of how vibrations travelled throughout the beam in space and time. Analysis of these plots could be used to determine which point of the blade experienced the greatest displacements in the vibrations post impact, suggesting likely locations where the blade might snap. The results show the greatest displacements in the vibrations occurred at the tip of the blade, the point of impact and near the root of the blade. These results may suggest the blade could undergo fracture in multiple places along the blade. Perhaps future work could involve a more robust combination of the static and dynamic models to evaluate where the blade would break. In addition, the importance of modelling the strength of the structure is clear, perhaps further work could be done on calculating the maximum force the structure could withstand in such an impact.

In conclusion, the modelling done throughout this report provides an insight into the outcome of a turbine blade toppling onto infrastructure, more specif ally whether the blade will break or not. However, collision modelling is a complicated topic in which many simplifying assumptions have been created to produce results. While this report has taken an analytic approach, companies concerned with the problem could use computer impact simulations to better determine the

damage such an impact would cause. Furthermore to produce more reliable results through an analytic approach, more realistic modelling of the turbine blade needs to be done.

References

[1] Cop26 goals. Accessed: 13/11/2021. https://ukcop26.org/cop26-goals/.

[2] Boris johnson: Wind farms could power every home by 2030. Accessed: 16/11/2021. https://www.bbc.co.uk/news/uk-politics-54421489.

[3] Wind energy in the uk. Accessed: 16/11/2021. https://www.ons.gov.uk/economy/environmentalaccounts/articles/windenergyintheuk/june2021.

[4] Onshore windfarm subsidies. Accessed: 9/11/2021. https://www.theguardian.com/business/2020/mar/02/uk-government-lifts-block-on-new-onshore-windfarm-subsidies.

[5] Bernard Stark. *Energy Management Workbook*. 2021.

[6] Why giant turbines are pushing the limits of possibility. Accessed: 11/11/2021. https://www.bbc.co.uk/news/business-58704792.

[7] P Baniotopoulos M Vazquez. Wind turbine tower collapse cases: A historical overview. *Structures and Buildings*, 172, 2019. https://doi.org/10.1680/jstbu.17.00167.

[8] Recent trends and future projections of uk storm activity. Accessed: 12/11/2021. https://www.metoffice.gov.uk/research/news/2021/recent-trends-and-future-projections-of-uk-storm-activity.

[9] J Mayer S Faulstich, V Berkhout and D Siebenlist. Modelling the failure behaviour of wind turbines. *Journal of physics*, 2016.

[10] B Le and J Andrews. Modelling wind turbine degradation and maintenance. *Nottingham Transportation Engineering Centre*, 2019.

[11] R Irving. Illustrative blade throw analysis for wind turbine failure. *M.ENG report*, page 52, 2021.

[12] MMI Engineering Ltd. Study and development of a methodology for the estimation of the risk and harm to persons from wind turbines. *CME*, 2013. https://www.hse.gov.uk/research/rrpdf/rr968.pdf.

[13] P Wriggers. *Computational Contact Mechanics*. John Wiley, Hannover, Germany, 2002.

[14] K.L Johnson. *Contact Mechanics*. University of Cambridge, Cambridge, 1985.

[15] J. D. Littell. Full-scale drop test of a fokker f28 wing-box fuselage section. *Structural Dynamics Branch*, 2017. https://ntrs.nasa.gov/api/citations/20180006305/downloads/20180006305.pdf.

[16] P J. Schubel and R J. Crossley. Wind turbine blade design. *Energies*, 2012.

[17] M Saravia. Calculation of the cross sectional properties of large wind turbine blades. *Faculty of technology of university of Bahía Blanca*, 2016.

[18] A D Garrad. Engineering clarifications of the ace wind turbine project. *ACE*, 2020.

[19] Wind watch faq — size. Accessed: 13/11/2021. https://www.wind-watch.org/faq-size.php.

[20] Loeriesfontein wind farm - wind turbine facts. Accessed: 20/12/2021. https://loeriesfonteinwind.co.za/wind-energy-library/wind-turbine-facts/#:~:text=Wind%20turbine%20blades%20rotate%20between,as%20much%20as%20120%2C000%20hours.

[21] G Kubo T Sakai and H Kubo. Theoretical considerations on estimation of compressive strength of concrete by means of hammer blowing. *Nitto Construction*. http://www.claisse.info/2013

[22] Timoshenko ehrenfest beam theory. Accessed: 27/02/2022. https://en.wikipedia.org/wiki/Timoshenko%E2%80%93Ehrenfest_beam_theory.

[23] Properties of e-fibre glass. Accessed: 9/11/2021. https://www.azom.com/properties.aspx?ArticleID=764.

[24] Stresses deflections in beams. Accessed: 13/02/2022. https://mechanicalc.com/reference/beam-analysis.

[25] Modeling of the mechanical properties of a wood-fiber/bicomponent-fiber composite. Accessed: 9/03/2022. https://bioresources.cnr.ncsu.edu/resources/modeling-of-the-mechanical-properties-of-a-wood-fiberbicomponent-fiber-composite/.

[26] Euler–bernoulli beam theory. Accessed: 22/12/2021. https://en.wikipedia.org/wiki/Euler%E2%80%93Bernoulli_beam_theory.